

Acoustophoretic Synchronization of Mammalian Cells in Microchannels

Patrick Thévoz,^{†,‡} Jonathan D. Adams,[§] Herbert Shea,[‡] Henrik Bruus,^{||} and H. Tom Soh^{*,†,⊥}

Department of Mechanical Engineering, University of California, Santa Barbara, California 93106, Microsystems for Space Technologies Laboratory, Ecole Polytechnique Fédérale de Lausanne (EPFL), CH-2002 Neuchâtel, Switzerland, Department of Physics, University of California, Santa Barbara, California 93106, Department of Micro- and Nanotechnology, Technical University of Denmark, DTU Nanotech Building 345 East, DK-2800 Kongens Lyngby, Denmark, and Materials Department, University of California, Santa Barbara, California 93106

We report the first use of ultrasonic standing waves to achieve cell cycle phase synchronization in mammalian cells in a high-throughput and reagent-free manner. The acoustophoretic cell synchronization (ACS) device utilizes volume-dependent acoustic radiation force within a microchannel to selectively purify target cells of desired phase from an asynchronous mixture based on cell cycle-dependent fluctuations in size. We show that ultrasonic separation allows for gentle, scalable, and label-free synchronization with high G₁ phase synchrony (~84%) and throughput (3 × 10⁶ cells/h per microchannel).

The capability to synchronize a population of asynchronous cells into a particular phase in their cell cycle is of paramount importance in biomedical research. For example, synchronization-based studies of cancer cells have enabled the discovery of cellular proliferation factors¹ and cell-cycle regulation factors.^{2,3} For cancer therapeutics development, achieving effective synchrony of tumor cell samples is critical to understanding their response to chemotherapeutics, because many anticancer drugs target cells in a particular phase.^{4,5} The cell cycle generally consists of four phases—G₁ (gap 1), S (synthesis), G₂ (gap 2), and M (mitosis)—and it is well-known that for almost all cell types, their size is highly correlated to their phase.^{6,7} Currently, the most prevalent method for cell synchronization is the chemical arrest and release technique,^{8–10} wherein cells are treated with metabolic agents that block the cell cycle at a particular point,

driving phase-specific accumulation, after which a second reagent is used to release the cells and thereby achieve synchrony. Though effective, this method suffers from a critical drawback in that it affects the physiology of the cells in ways that could undermine their usefulness as accurate models of normal cellular events.^{11,12} Centrifugal elutriation^{9,13} offers a less invasive approach,¹⁴ but it requires time-consuming sample preparation, suffers from low throughput, and imposes mechanical stress on the cells.¹⁵

Microfluidics technology offers a promising alternative to conventional methods of cell synchronization because it allows accurate control of fluidic and separation forces in a reproducible manner.¹⁶ Recent efforts have explored a number of different separation forces in microchannels for cell synchronization, including dielectrophoresis¹⁷ and hydrophoresis,¹⁸ but the low throughput of both approaches (<400 μL/h, ~2.5 × 10⁵ cells/h per microchannel) have limited their utility. In an effort to develop a noninvasive, high purity method that can also operate at a higher throughput, we report here the first use of ultrasonic standing waves for cell synchronization. The acoustophoretic cell synchronization (ACS) device uses a volume-dependent acoustic radiation force to isolate and purify mammalian cells based on cell-cycle phase into independent outlets at both high G₁ phase synchrony (~84%) and high throughput (3 × 10⁶ cells/h per microchannel).

MATERIALS AND METHODS

Device Fabrication. Standard microfabrication techniques were used to fabricate the ACS device. Briefly, a 500-μm-thick, 100-mm-diameter silicon wafer was coated with a 1.4-μm-thick layer of AZ5214E-IR negative photoresist (Clariant, Somerville, NJ). Standard photolithography was utilized to pattern the microchannels. The channels were etched to a depth of 50 μm using the Bosch deep reactive-ion etching process (770 SLR, Plas-

* To whom correspondence should be addressed. E-mail: tsoh@engineering.ucsb.edu.

[†] Department of Mechanical Engineering, University of California.

[‡] Ecole Polytechnique Fédérale de Lausanne (EPFL).

[§] Department of Physics, University of California.

^{||} Technical University of Denmark.

[⊥] Materials Department, University of California.

- (1) Nagel, W. W.; Vallee, B. L. *Proc. Natl. Acad. Sci. U.S.A.* **1995**, *92*, 579–583.
- (2) Hartwell, L. H.; Kastan, M. B. *Science* **1994**, *266*, 1821–1828.
- (3) Hunter, T.; Pines, J. *Cell* **1994**, *79*, 573–582.
- (4) Jolivet, J.; Cowan, K. H.; Curt, G. A.; Clendeninn, N. J.; Chabner, B. A. *N. Engl. J. Med.* **1983**, *309*, 1094–1104.
- (5) Schiff, P. B.; Fant, J.; Horwitz, S. B. *Nature* **1979**, *277*, 665–667.
- (6) Jorgensen, P.; Tyers, M. *Curr. Biol.* **2004**, *14*, R1014–R1027.
- (7) Ramirez, O. T.; Mutharasan, R. *Biotechnol. Bioeng.* **1990**, *36*, 839–848.
- (8) Jackman, J.; O'Connor, P. M. *Curr. Prot. Cell Biol.* **1998**, 8.3.18.3.20.
- (9) Davis, P. K.; Ho, A.; Dowdy, S. F. *Biotechniques* **2001**, *30*, 1322–1324.
- (10) Kumagai-Sano, F.; Hayashi, T.; Sano, T.; Hasezawa, S. *Nat. Protoc.* **2006**, *1*, 2621–2627.

- (11) Ji, C.; Marnett, L. J.; Pietenpol, J. A. *Oncogene* **1997**, *15*, 2749–2753.
- (12) Cooper, S. *Cell. Mol. Life Sci.* **2003**, *60*, 1099–1106.
- (13) Banfalvi, G. *Nat. Protoc.* **2008**, *3*, 663–673.
- (14) Zickert, P.; Wejde, J.; Skog, S.; Zetterberg, A.; Larsson, O. *Exp. Cell Res.* **1993**, *207*, 115–121.
- (15) Hohmann, L. K.; Shows, T. B. *Somatic Cell Genet.* **1979**, *5*, 1013–1029.
- (16) Adams, J. D.; Kim, U.; Soh, H. T. *Proc. Natl. Acad. Sci. U.S.A.* **2008**, *105*, 18165–18170.
- (17) Kim, U.; Shu, C. W.; Dane, K. Y.; Daugherty, P. S.; Wang, J. Y. J.; Soh, H. T. *Proc. Natl. Acad. Sci. U.S.A.* **2007**, *104*, 20708–20712.
- (18) Choi, S.; Song, S.; Choi, C.; Park, J. K. *Anal. Chem.* **2009**, *81*, 1964–1968.

matherm, St. Petersburg, FL) using photoresist as a mask. After stripping the photoresist, inlet and outlet access holes were drilled using a CNC drill (Flashcut CNC, Deerfield, IL) equipped with a 1.1-mm-diameter diamond bit (Triple Ripple, Abrasive Technology, Lewis Center, OH). The wafers were subsequently diced using a semiautomatic dicing saw (Disco, Tokyo, Japan). A borofloat glass lid was then anodically bonded onto the silicon chip by applying a 1000 V bias at 375 °C for 5 min (SB6, Suss Microtec AG, Garching, Germany). Finally, inlet and outlet tubing were glued to the device with 5 min epoxy (Devcon, Danvers, MA), and the piezoactuator (26051, Ferroperm Piezoceramics, Kvistgaard, Denmark) was attached to the silicon side of the device with superglue (Ross Super Glue Gel, Elmer's Products, Inc., Columbus, OH).

Numerical Simulation. At sufficiently low concentrations, the hydrodynamic interaction between cells or particles does not significantly impact their motion in microfluidic systems.¹⁹ We therefore used a simplified single-particle acoustophoretic model to simulate the particle motion in the ACS device. More specifically, in the direction transverse to the flow (i.e., *y*-direction), the acoustic radiation force $F_{ac}(y)$ is balanced by the viscous Stokes drag $F_{drag} = 6\pi\eta a \, dy/dt$ for a spherical particle of radius *a*, where η is the viscosity of the medium. If we furthermore make the approximation that the flow velocity along the channel is constant and equal to its mean value, the resulting differential equation $F_{ac}(y) = 6\pi\eta a \, dy/dt$ can be integrated to yield an expression for the transverse position $y(t)$ of a particle in the ultrasound field as a function of time t ,²⁰

$$y(t) = \frac{1}{k_y} \arctan\left\{\tan[k_y y(0)] \exp\left[\frac{\Phi}{\eta} (2k_y a)^2 \langle E_{ac} \rangle t\right]\right\} \quad (1)$$

Here $y(0)$ is the starting position of the particle of radius *a*, $k_y = 2\pi/\lambda$ is the wavenumber, and $\langle E_{ac} \rangle$ is the time-averaged energy density of the ultrasound wave of wavelength λ inside the channel. Notably, the $a^2 t$ factor in eq 1 governs the relationship between particle volume and the necessary time to focus the particle into a particular flow stream. This formula was used to model the trajectories of particles of different sizes. We found that it was sufficient to plot the paths of the outermost and innermost particle in each band at the inlets, because the paths of all other particle paths fell in between these extremes.

Bead Separation. Red fluorescent 2- μ m-diameter and green fluorescent 5- μ m-diameter polystyrene beads (R0200 and G0500, Duke Scientific, Fremont, CA) were suspended in ultrapure water to form a mixture with a total concentration of 0.5×10^9 beads/mL. For separation, a 2.044 MHz 30 V_{pp} sinusoidal signal was applied to the ultrasonic transducer. The bead mixture and buffer flow, consisting of ultrapure water, were injected into the ACS device at flow rates of 3 and 6 mL/h, respectively, via dual programmable syringe pumps (PhD 2000, Harvard Apparatus, Holliston, MA). Outlet fractions were collected in microcentrifuge tubes and subsequently analyzed via flow cytometry (FACSaria, BD Biosciences, San Jose, CA). Following bead separation, the device was rinsed thoroughly with ultrapure water.

Cell Preparation and Separation. MDA-MB-231 cells were cultured at 37 °C and 5% CO₂ in Dulbecco's Modified Eagle's Medium (DMEM) supplemented with 10% fetal bovine serum (FBS) and 1% penicillin-streptomycin. Cells were harvested from the culture dish with 0.05% trypsin-EDTA before reaching 70% confluency, to avoid abnormal cell sizes due to confinement. All cell culture media and reagents were purchased from ATCC (Manassas, VA).

Harvested cells were pelleted and resuspended at a concentration of approximately 1.2×10^6 cells/mL in a 1 \times phosphate buffered saline (PBS) solution containing 2% bovine serum albumin (BSA) (Fraction V, Sigma-Aldrich, St. Louis, MO) and 1 mM EDTA (Sigma-Aldrich, St. Louis, MO) to avoid cell adhesion and the formation of aggregates. The cell mixture and buffer (also 1 \times PBS, 2% BSA, 1 mM EDTA) were injected into the device via at flow rates of 3 and 6 mL/h, respectively, and a sinusoidal signal at 2.044 MHz was applied to the piezoactuator. To account for the different focusing rate of the cells versus the beads, the signal amplitude was set to 11.6 V_{pp} . Because the actuation frequency determines the induced pressure field, the shape of the acoustic field was not altered compared with the bead experiments. The device was monitored during operation using an inverted microscope (TE2000-S, Nikon Inc., Melville, NY) connected to a CCD camera (CoolSNAP HQ₂, Photometrics, Tuscon, AZ). To help reduce cell loss, sample inlet tubing was oriented vertically and leading directly into the device. A small amount of cell adhesion to the walls of the device was observed, chiefly at the fork between the separation channel and the outlet channels. Outlet fractions were collected in microcentrifuge tubes during separation. Following cell separation, the device was cleaned with a solution of 10% bleach, followed by thorough rinsing with ultrapure water.

Propidium Iodide Staining and FACS Analysis. The cell cycle populations were determined by analyzing the cellular DNA content via propidium iodide DNA staining and flow cytometry.²¹ After synchronizing the cells in the ACS device, the collected cell fractions were pelleted and resuspended in 200 μ L of 1 \times PBS, then fixed in 70% ethanol on ice for at least 2 h. Fixed cells were then centrifuged at 650g for 8 min and resuspended in 200 μ L of staining solution (1 \times PBS, 0.1% vol/vol Triton X-100, 200 μ g/mL RNase A and 10 μ g/mL propidium iodide, a DNA-intercalating dye²¹). Cells were incubated for 30 min at room temperature and subsequently analyzed with flow cytometry. Cell cycle populations were obtained from the data using ModFit LT DNA cell-cycle analysis software (Verity Software House, Topsham, ME).

RESULTS AND DISCUSSIONS

As described in seminal work by Laurell and co-workers,^{22–25} microfluidic acoustophoresis operates by generating an ultrasonic standing wave (typically in the 0.1–10 MHz range) that imposes

(21) Darzynkiewicz, Z.; Juan, G.; Bedner, E. *Curr. Prot. Cell Biol.* **2001**, 8.4.18.4.18.

(22) Laurell, T.; Petersson, F.; Nilsson, A. *Chem. Soc. Rev.* **2007**, 36, 492–506.
(23) Nilsson, A.; Petersson, F.; Jonsson, H.; Laurell, T. *Lab Chip* **2004**, 4, 131–135.

(24) Petersson, F.; Aberg, L.; Sward-Nilsson, A.-M.; Laurell, T. *Anal. Chem.* **2007**, 79, 5117–5123.

(25) Petersson, F.; Nilsson, A.; Holm, C.; Jonsson, H.; Laurell, T. *Lab Chip* **2005**, 5, 20–22.

(19) Mikkelsen, C.; Bruus, H. *Lab Chip* **2005**, 5, 1293–1297.

(20) Barnkob, R.; Augustsson, P.; Laurell, T.; Bruus, H. *Lab Chip* **2010**, 10, 563–570.

an acoustic radiation force on the cells such that they are attracted toward the nodes or antinodes of the standing pressure wave. More specifically, the acoustic radiation force F_{ac} in the transverse y -direction can be approximated by

$$F_{ac} = -\frac{\pi p_1^2 V \beta_0}{2\lambda} \phi(\beta, \rho) \sin\left(\frac{4\pi y}{\lambda}\right) \quad (2)$$

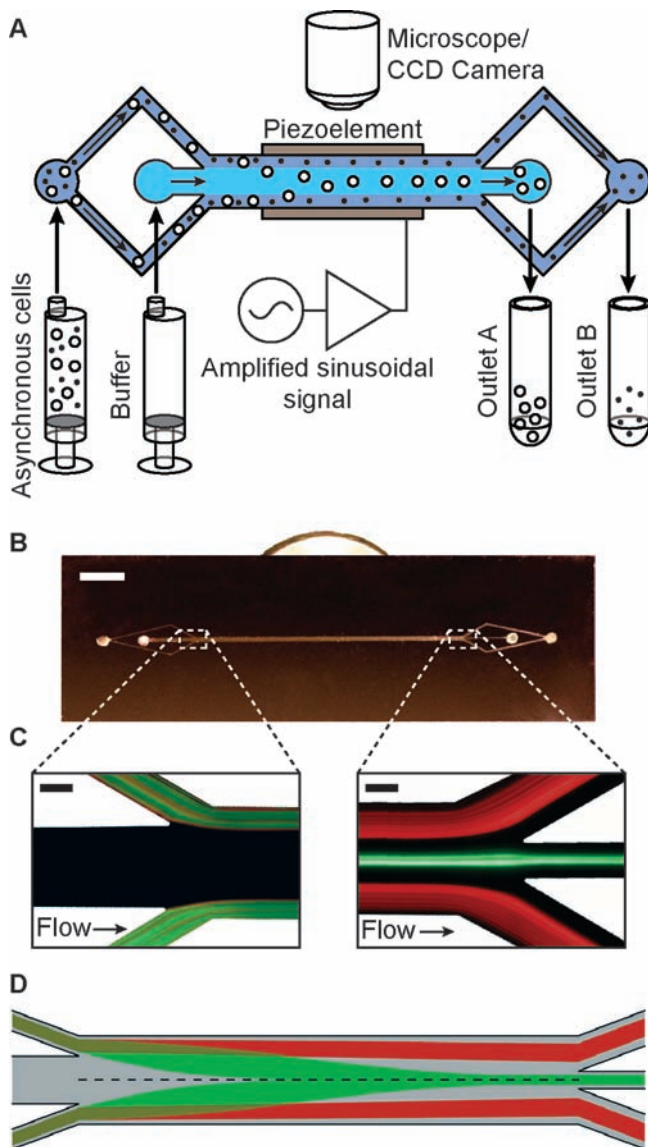


Figure 1. Acoustophoretic cell synchronization (ACS) device and experimental setup. (A) Asynchronous mixture of cells and buffer volumetrically pumped into the ACS device. Synchronization is achieved by fractionating the cells according to size such that larger cells (e.g., G_2) elute through outlet A whereas smaller cells (e.g., G_1) elute through outlet B. (B) Photograph of the device with attached piezoactuator on its backside (scale bar = 5 mm). (C) Fluorescence micrographs of the ACS device in operation. A binary mixture of green (5- μm -diameter) and red (2- μm -diameter) polystyrene beads enters the inlet area (left) and are acoustophoretically separated to elute through outlet 1 and 2, respectively (right). Scale bars are 50 μm in both images. (D) Two-dimensional numerical simulation of separation along the channel, showing buffer (gray) with bands of particle trajectories. Larger particles (green) are subject to a greater acoustic radiation force and thus converge faster to the nodal plane at the center of the channel (dashed line) and elute through outlet A. Smaller particles (red) do not reach the nodal plane and elute through outlet B.

with the contrast factor $\phi(\beta, \rho)$ defined as $\phi(\beta, \rho) = (5\rho_p - 2\rho_0) / (2\rho_p + \rho_0) - \beta_p/\beta_0$, where p_1 is the ultrasonic pressure amplitude; λ is the wavelength of the standing wave; V is the volume, ρ_p is the density; β_p is the compressibility of the cell; and ρ_0 and β_0 are the density and compressibility, respectively, of the suspension medium. From eq 2, it is apparent that the acoustophoretic force strongly depends on the transverse dimension of the separation channel and the volume of the cell, as well as the cell density and compressibility with respect to the suspension medium.

The acoustophoretic cell synchronization (ACS) device was designed to exploit this volume-dependent force to purify cells in a particular phase from an asynchronous mixture, such that they are eluted into independent outlets (Figure 1A). The acoustic standing waves are generated in the 3-cm-long, 350- μm -wide, and 50- μm -deep separation channel within the ACS device (Figure 1B), which is patterned in a silicon substrate and sealed with a glass cap. Sample and buffer solutions are injected with two independent syringe pumps, and the piezoelectric ultrasonic transducer is attached to the backside of the device and driven by amplifier circuitry based on an LT1210 operational amplifier (Linear Technologies, Milpitas, CA) and a radiofrequency function generator (33120A, Hewlett-Packard, Palo Alto, CA). The thickness of the piezoactuator was chosen such that its resonant frequency matched the fundamental harmonic of the standing pressure wave in the microchannel (~ 2 MHz).

Without piezoactuation, the low Reynolds number fluidic conditions ($Re \sim 13$) generate a steady laminar flow consisting of two peripheral sample streams and one central buffer stream within the microchannel (Figure 1C, left). When the piezotransducer is actuated, the stronger acoustic radiation force on larger cells (e.g., those in G_2/M and S phases) directs them to the central stream more rapidly compared to smaller cells (e.g., those in the G_1 phase), thereby allowing efficient separation at the outlets (Figure 1C, right). Quantitatively, assuming two cells (a and b) of different sizes but possessing the same density and compressibility, the relationship between the their volumes

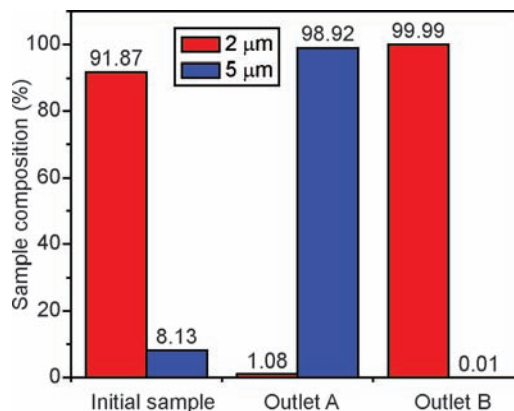


Figure 2. Validation study through separation of beads. A mixture of 2 and 5 μm polystyrene beads were separated in the ACS device at a sample flow rate of 3 mL/h. Flow cytometry analysis shows that the initial mixture consisted of 91.87% 2- μm beads (red) and 8.13% 5- μm beads (green). After a single pass through the ACS device, the sample retrieved from outlet A contained 98.92% 5- μm beads and that from outlet B contained 99.99% 2- μm beads.

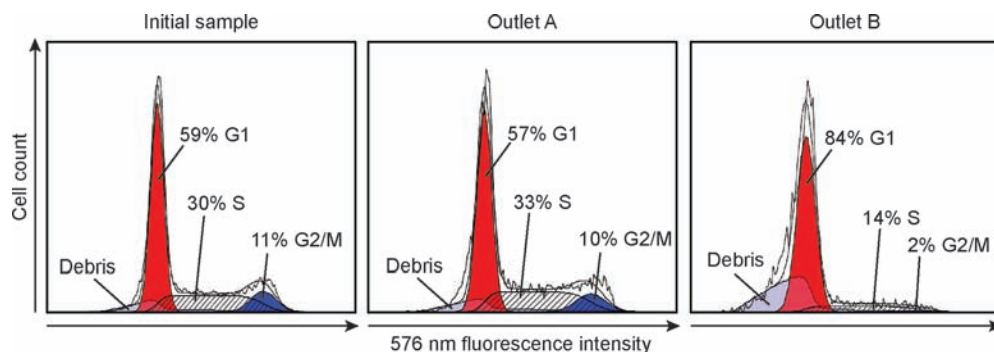


Figure 3. Flow cytometry histograms showing cell cycle distributions before and after synchronization, based on measurements of red fluorescence (centered at 576 nm) after staining the cellular DNA with propidium iodide. The populations in each phase of the cell cycle were determined by fitting cell cycle models to the histograms (ModFit LT). The synchronized cell population at outlet B shows 84% of all cells in the G_1 phase, with 14% in the S phase and 2% in G_2/M phase.

(V_a and V_b) and the required duration for them to focus at a node (τ_a and τ_b) can be expressed as

$$\frac{\tau_a}{\tau_b} = \left[\frac{V_b}{V_a} \right]^{2/3} \quad (3)$$

On the basis of this relationship, the channel geometry and the flow rates were chosen such that larger G_2/M and S phase cells elute through outlet A and smaller G_1 phase cells elute through outlet B (Figure 1D).

To validate the operating conditions, the ACS device was first characterized with two kinds of fluorescent polystyrene beads, 2 (red) and 5 μm (green) in diameter. The initial sample contained a binary mixture of red (91.87%) and green (8.13%) beads as measured with flow cytometry (Figure 2). We note that this ratio of beads was chosen to mimic the typical proportion of mammalian cells in the G_1 and G_2 phases.^{17,18} By monitoring bead separation while adjusting the piezo driving signal, the optimum operational frequency for the device was found to be 2.044 MHz. After a single pass through the device at a sample flow rate of 3 mL/h (1.5×10^9 beads/h), flow cytometry data shows highly efficient, label-free, size-based separation: 98.92% of green beads eluted through outlet A and 99.99% of red beads eluted through outlet B (Figure 2).

The MDA-MB-231 human breast ductal carcinoma cell line was used as a model for mammalian cell synchronization. Via optical microscopy, we confirmed that their size is highly correlated with their phase; we found that cells typically have a volume of $\sim 400 \mu\text{m}^3$ in the early G_1 phase, reaching approximately twice that volume when entering the G_2/M phase (data not shown). Studies of variations in the cell density throughout the cell cycle of representative mammalian cells are minor (<2%) and would not significantly affect the acoustic separation.^{26,27} The distribution of elastic coefficients (i.e., compressibility) is wider with change in mean value of up to 20% through the cell cycle.²⁸ However, such variability would have significantly smaller impact on the acoustic forces than the volume doubling through the cell cycle. Thus, assuming constant density ρ_p and compressibility

β_p , eq 3 predicts that cells in G_2/M phase will move toward the central node approximately 1.6 times faster than those in G_1 phase (i.e., $\tau_{G_2/M} < \tau_{G_1}$). On the basis of these calculations, the ACS device was configured to enrich G_1 cells in outlet B and deplete those in S and G_2/M phases via outlet A. This configuration was chosen because the duration of G_1 (~ 16 – 24 h) is significantly longer than G_2/M (2.5–3 h), reducing the probability that cells will undergo division during operation. Cells were separated at a sample throughput of 3 mL/h (3×10^6 cells/h). Compared with the bead validation experiment, the concentration is reduced to limit the presence of cellular aggregates, and no significant difference in separation performance was observed for a wide range of concentrations of beads (Supporting Information Figure 1).

To determine cell cycle phase after separation, the collected cells were fixed and stained with propidium iodide and analyzed with flow cytometry, and the resulting histograms were modeled using ModFit LT DNA cell cycle analysis software. The number of cells modeled in each histogram was 21 115, 9739, and 4399, for the initial, outlet A, and outlet B samples, respectively. Before separation, the distribution of G_1 , S, and G_2/M cells in the sample population was 59%, 30%, and 11%, respectively, which is consistent with the residence time in their respective phases and with previously reported values (Figure 3, initial sample).^{29,30} After a single pass through the device, in outlet A, the population of G_1 , S, and G_2/M cells was 57%, 33%, and 10%, respectively (Figure 3, outlet A), while at outlet B the population was 84% G_1 , 14% S, and 2% G_2/M phase cells (Figure 3, outlet B), or 84% G_1 phase synchrony. We note that to elute only G_1 cells out of outlet B, we are necessarily biasing our selection toward only the smallest cells from the early part of the G_1 phase. Thus, although many late-stage cells in the G_1 phase elute through outlet A, a high level of G_1 phase synchrony at outlet B may be achieved.

The effect of acoustophoretic separation on cell viability was investigated via trypan blue-based dye exclusion experiments immediately after separation (Supporting Information Figure 2) and through long-term reculturing of cells collected after separa-

(26) Loken, M. R.; Kubitschek, H. E. *J. Cell. Physiol.* **1984**, *118*, 22–26.

(27) Anderson, E. C.; Petersen, D. F.; Tobey, R. A. *Biophys. J.* **1970**, *10*, 630–645.

(28) Zhang, G.; Long, M.; Wu, Z. Z.; Yu, W. Q. *World J. Gastroent.* **2002**, *8*, 243–246.

(29) Pervin, S.; Singh, R.; Chaudhuri, G. *Proc. Natl. Acad. Sci. U.S.A.* **2001**, *98*, 3583–3588.

(30) Li, Z.; Li, J.; Mo, B.; Hu, C.; Liu, H.; Qi, H.; Wang, X.; Xu, J. *Cell Biol. Toxicol.* **2008**, *24*, 401–409.

tion (Supporting Information Figure 3). Consistent with previous literature,³¹ both experiment revealed no significant change in the viability of cells, presumably due to the brief (~200 ms) ultrasound exposure.

CONCLUSIONS

We report the first use of ultrasonic standing waves to achieve cell synchronization. The device performance benefited specifically from the use of microfluidic channels that enable accurate, efficient, and reproducible establishment of a volume-dependent ultrasonic separation force, as well as multistream laminar-flow architecture for high purity separation. We note that our method offers throughput that is approximately an order of magnitude higher than previous microfluidic approaches in both volumetric and cell throughputs,^{17,18} and appears to have negligible impact on cell viability. In comparison with conventional techniques, the ACS device achieves comparable levels of G₁ phase synchrony. For example, various chemical arrest techniques for MDA-MB-231 cells reported purities of individual cell cycle populations of order 85–90% for G₁ phase arrest,^{29,32} while centrifugal elutriation can achieve up to 90–95% G₁ phase synchrony.³³ We

(31) Hultstrom, J.; Manneberg, O.; Dopf, K.; Hertz, H. M.; Brismar, H.; Wiklund, M. *Ultrasound Med. Biol.* **2007**, *33*, 145–151.

(32) Barascu, A.; Besson, P.; Le Floch, O.; Bougnoux, P.; Jourdan, M. L. *Int. J. Biochem. Cell. B* **2006**, *38*, 196–208.

(33) Wahl, A. F.; Donaldson, K. L. *Curr. Prot. Cell Biol.* **1999**, 8.5.18.5.16.

(34) Bessette, P. H.; Hu, X.; Soh, H. T.; Daugherty, P. S. *Anal. Chem.* **2007**, *79*, 2174–2178.

believe higher purities and higher throughput should be achievable through serial integration of the device,³⁴ through optimization of channel geometry, and through parallel operation.²² Finally, given that acoustophoresis allows the use of a wide range of cells and suspension media, we believe our approach represents a promising, universal approach for low-stress and label-free cell synchronization with high throughput and fidelity.

ACKNOWLEDGMENT

The authors thank Patrick S. Daugherty for the kind gift of the mammalian cells, Unyoung Kim and Jinpeng Wang for help with flow cytometry, and Seung-Soo Oh and B. Scott Ferguson for help with cell culturing. We thank the ONR, NIH, ARO Institute for Collaborative Biotechnologies (ICB), and Armed Forces Institute for Regenerative Medicine (AFIRM) for their financial support. Microfabrication was carried out in the Nanofabrication Facility at UC Santa Barbara. P.T. and J.D.A. contributed equally to this work.

SUPPORTING INFORMATION AVAILABLE

Supplementary Figures 1–3. This material is available free of charge via the Internet at <http://pubs.acs.org>.

Received for review February 8, 2010. Accepted February 10, 2010.

AC100357U